Supporting Information

Shannon et al. 10.1073/pnas.1212647110

SI Text

Uncertainty Analysis of Speedup Observations

Uncertainty in the speedup has been calculated from the measurement error in the velocity observations. For the University of Edinburgh/University of Aberdeen data, the error in the annual velocity δv is 5.6 m·y^{-1} (1). This is a conservative error estimate representing noise in the global positioning system (GPS) signal.

The annual error is a function of the monthly velocity errors

$$\delta v = \sqrt{\sum_{i=1}^{12} v_i^2},$$

where i refers to month from January to December. If we assume each month has the same error, then the monthly error δv_i is

$$\delta v_i = \frac{\delta v}{\sqrt{12}}$$

or $\delta v_i = 1.62$ m·y^{-1}. The error in the mean velocity of the lowest three months δv_3 is

$$\delta v_3 = \sqrt{3\delta v_i^2}$$

or $\delta v_3 = 2.8$ m·y^{-1}. The error in the speedup δS is calculated using the rule for the propagation of errors when doing division,

$$\frac{\delta S}{S} = \sqrt{\left(\frac{\delta v}{\bar{v}}\right)^2 + \left(\frac{\delta v_3}{\bar{v}_3}\right)^2},$$

where S is the speedup, $\bar{v}$ is the annual velocity, and $\bar{v}_3$ is the mean velocity of the lowest three monthly velocities.

The measurement error in the Utrecht University data is described in ref. 2. More specifically, hourly measurements of the position are averaged without weighting functions over 168 data points, yielding an uncertainty of 0.27 m in the position of a fixed point. This results in an uncertainty of 0.81 m·y^{-1} for monthly values and, by following equations 3 and 4, in 1.40 m·y^{-1} for three-month velocities and 2.75 m·y^{-1} for annual velocities.

Further Analysis of the Relation Between Runoff and Speedup

To investigate the trend seen in Fig. 2, a linear regression line was fitted at each field site individually between the speedup and runoff. The gradients of the speedup are shown in Fig. S1. A positive gradient is seen at sites 4, 5, 6, SHR, and S6; a negative gradient at sites 2 and S4; and no change at sites 1 and 3. It is unclear whether these latter sites flip from cavity to channelized drainage as runoff increases or whether they are truly uncoupled from the hydrological system. Sites 7 and S10 are omitted because they have no runoff according to the Modèle Atmosphérique Régional (MAR). Fig. S1 suggests that the gradient of the relation between speedup and runoff falls with increasing runoff and becomes negative at runoff above 1.2 m·y^{-1}.

Description of Ice Sheet Models

Vrije Universiteit Brussel Greenland Ice Sheet Model (VUB-GISM-HO). VUB-GISM-HO is a higher-order 3D, thermomechanical ice-flow model (3, 4) modified and extended for projections on centennial timescales. The higher-order approximation to the force balance accounts for horizontal gradients of membrane stresses that allow for inland transmission of perturbations at the ice-sheet margin in a more realistic way (5, 6). The model is implemented on a horizontal grid of 5-km resolution with 30 nonequidistant layers in the vertical. Ice temperature is prescribed and does not evolve over time. Isostatic bedrock adjustment is disabled. The model is initialized close to the present-day observed geometry and applies a synthetic mass balance correction to avoid model drift. A detailed description of the model, the initialization procedure, and the model sensitivity is given in ref. 7. The model simulates the internal distribution of temperature within the ice sheet so that the spatial extent of ice that is frozen to bedrock is known; in these areas (limited to the central regions of the ice sheet) ice velocity is assumed not to change in response to variations in runoff.

Elmer/Ice. Elmer/Ice builds on Elmer, the open-source, parallel, finite-element code, mainly developed by the CSC-IT Center for Science in Finland. Elmer/Ice solves for the transient full-Stokes system, using a 3D, vertically extruded, unstructured mesh in the horizontal plane. This method allows horizontal grid size smaller than 1 km for individual outlets. The model is run in parallel, using a 48-partition mesh. In this application, the ocean water pressure is imposed on the margin of the ice sheet, which is not allowed to move horizontally. Ice temperature is prescribed from the shallow-ice model Simulation Code for Polythermal Ice Sheets (SICOPOLIS) (8) and does not evolve over time. The initial state is constructed using a control inverse method (9) to infer the basal drag from the observed surface velocities (10) and ice-sheet topography. The upper surface is then allowed to relax during a 55-y period forced by a constant climate given by the 1989–2008 means for Equipe de Recherche Associée (ERA)-interim–forced MAR. The end of the relaxation period constitutes the initial state of prognostic experiments.

In the experiments, annual-mean surface mass balance (SMB) anomalies are added to these ERA-interim–forced MAR 1989–2008 means. Additional experiments [a run with only SMB forcing (SMBONLY), MAR-European Centre Hamburg Model (ECHAM5), E1, and A1B] with a synthetic mass balance (to avoid model drift) show an additional 3- to 4-mm sea-level rise (SLR) compared with experiments with control bias added. Details of the model and the initialization procedure can be found in ref. 11.

Community Ice Sheet Model 2.0. The Community Ice Sheet Model (CISM) version 2.0 includes improvements to all components of the original, shallow-ice approximation Glimmer-CISM model (12). The momentum balance is based on the 3D, first-order approximation to the Stokes equations (13). Mass, temperature, and general "tracer" advection take advantage of incremental remapping (14). All model components are fully parallel and scale to order ~1,000 processors (15). Model numerics, including nonlinear (Picard and Newton-based) solution methods, are discussed in ref. 16. Sliding is generally treated using a linear-viscous sliding law. A similar, large-scale application of the model to the Greenland ice sheet (GrIS) is described in ref. 17.

Model initialization for the current set of experiments involves a quasi-steady-state thermal spin-up, using surface temperature and geothermal flux fields taken from the SeaRISE datasets for Greenland (http://websrv.cs.umt.edu/isis/index.php/Present_Day_Greenland). As part of the initialization procedure, basal sliding

is tuned to match balance velocities. The tuned, initial condition implies a "synthetic" SMB field, which is applied for the control run and used as the base upon which SMB anomalies are applied for runs with climate forcing. Additional information on model initialization and tuning procedures can be found in the supporting information of ref. 17.

Model for Prediction Across Scales–Land Ice. The Model for Prediction Across Scales (MPAS)-Land Ice model is based on the MPAS climate-modeling framework of ref. 18. MPAS defines centroidal-Voronoi-tesselation (CVT)–based, variable-resolution meshes and includes a suite of standard model operators (e.g., high-order accurate advection routines), using finite-volume methods on a computational C-grid. The momentum balance is based on the 3D first-order approximation to the Stokes equations (13), implemented using continuous finite-element methods (FEM) on an unstructured, 3D mesh [obtained by vertically extruding the 2D, dual mesh to the MPAS CVT (i.e., a Delaunay triangulation)]. The model and FEM discretization, described in ref. 19, use the LifeV library (www.lifev.org).

For the current set of experiments, the model uses a fixed, uniform, ∼5-km resolution hexagonal mesh with 10 layers in the vertical. A first-order upwinding scheme is used for mass advection. Internal temperature fields are taken from the CISM initial condition (described above) and held constant and steady for the duration of the 200-y simulations. Basal sliding parameters are also taken from the CISM initialization and either held constant and steady in time (for the control and surface-mass-balance–forcing-only simulations) or modified according to the lubrication parameterizations discussed in the main text. MPAS-Land Ice simulations apply their own synthetic SMB and anomaly forcing, as described above for CISM simulations.

The Response of All of the Ice Sheet Models

The responses of VUB-GISM-HO, Elmer/Ice, and MPAS-Land Ice are shown in Figs. S2–S4, respectively.

1. Bartholomew I, et al. (2011) Seasonal variations in Greenland Ice Sheet motion: Inland extent and behaviour at higher elevations. *Earth Planet Sci Lett* 307:271–278.
2. den Ouden MAG, Reijmer CH, Pohjola V, van de Wal RSW, Oerlemans J (2010) Ice-velocity observations using a single-frequency GPS on Nordenski öldbreen, Svalbard. *Cryosphere* 4:593–604.
3. Huybrechts P (2002) Sea-level changes at the LGM from ice-dynamic reconstructions of the Greenland and Antarctic ice sheets during the glacial cycles. *Quat Sci Rev* 21:203–231.
4. Huybrechts P, De Wolde J (1999) The dynamic response of the Greenland and Antarctic ice sheets to multiple-century climatic warming. *J Clim* 12(8):2169–2188.
5. Fürst JJ, et al. (2011) Improved convergence and stability properties in a three-dimensional higher-order ice sheet model. *Geosci Model Dev* 4:1133–1149.
6. Fürst JJ, Goelzer H, Huybrechts P (2013) Effect of higher-order stress gradients on the centennial mass evolution of the Greenland ice sheet. *Cryosphere* 7(1):183–199.
7. Goelzer H, et al. Sensitivity of Greenland ice sheet projections to model formulations. *J Glaciol* 59(216):733–749.
8. Greve R (1997) Application of a polythermal three-dimensional ice sheet model to the Greenland ice-sheet: Response to steady-state and transient climate scenarios. *J Clim* 10:901–918.
9. Morlighem M, et al. (2010) Spatial patterns of basal drag inferred using control methods from a full-Stokes and simpler models for Pine Island Glacier, West Antarctica. *Geophys Res Lett* 37:6.
10. Joughin I, Smith BE, Howat IM, Scambos T, Moon T (2010) Greenland flow variability from ice-sheet-wide velocity mapping. *J Glaciol* 56:415–430.
11. Gillet-Chaulet F, et al. (2012) Greenland Ice Sheet contribution to sea-level rise from a new-generation ice-sheet model. *Cryosphere* 6:1561–1576.
12. Rutt I, Hagdorn M, Hulton N, Payne A (2009) The "Glimmer"community ice sheet model. *J Geophys Res* 114:F02004.
13. Pattyn F (2003) A new three-dimensional higher-order thermomechanical ice sheet model: Basic sensitivity, ice stream development, and ice flow across subglacial lakes. *J Geophys Res* 108(2382):B8.
14. Dukowicz J, Baumgardner J (2000) Incremental remapping as a transport/advection algorithm. *J Comput Phys* 160:318–335.
15. Evans KJ, et al. (2012) A modern solver interface to manage solution algorithms in the Community Earth System Model. *Int J High Performance Comput* 26(1):54–62.
16. Lemieux JF, et al. (2011) Implementation of the Jacobian-free Newton-Krylov method for solving the first-order ice sheet momentum balance. *J Comput Phys* 230: 6531–6545.
17. Price SF, Payne AJ, Howat IM, Smith BE (2011) Committed sea-level rise for the next century from Greenland ice sheet dynamics during the past decade. *Proc Natl Acad Sci USA* 108(22):8978–8983.
18. Ringler T, Ju L, Gunzburger M (2008) A multiresolution method for climate system modeling: Application of spherical centroidal Voronoi tessellations. *Ocean Dyn* 58(5-6):475–498.
19. Perego M, Gunzburger M, Burkardt J (2012) Parallel finite-element implementation for higher-order ice-sheet models. *J Glaciol* 58(207):76–88.

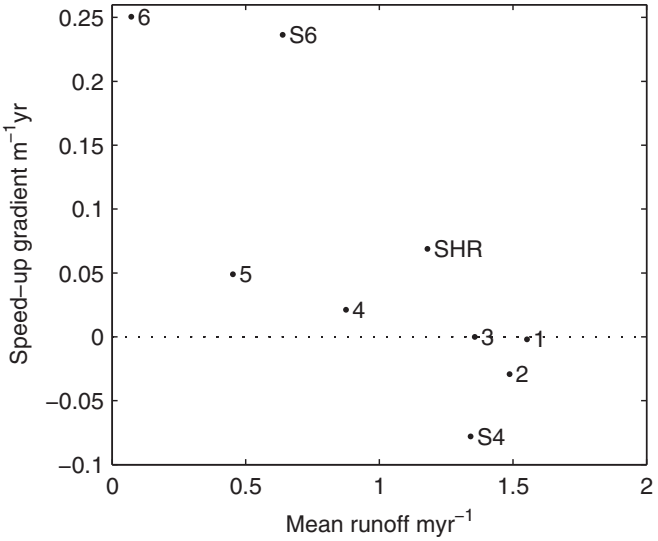

Fig. S1. Gradient of a linear regression between annual speedup and annual mean runoff for each field site.

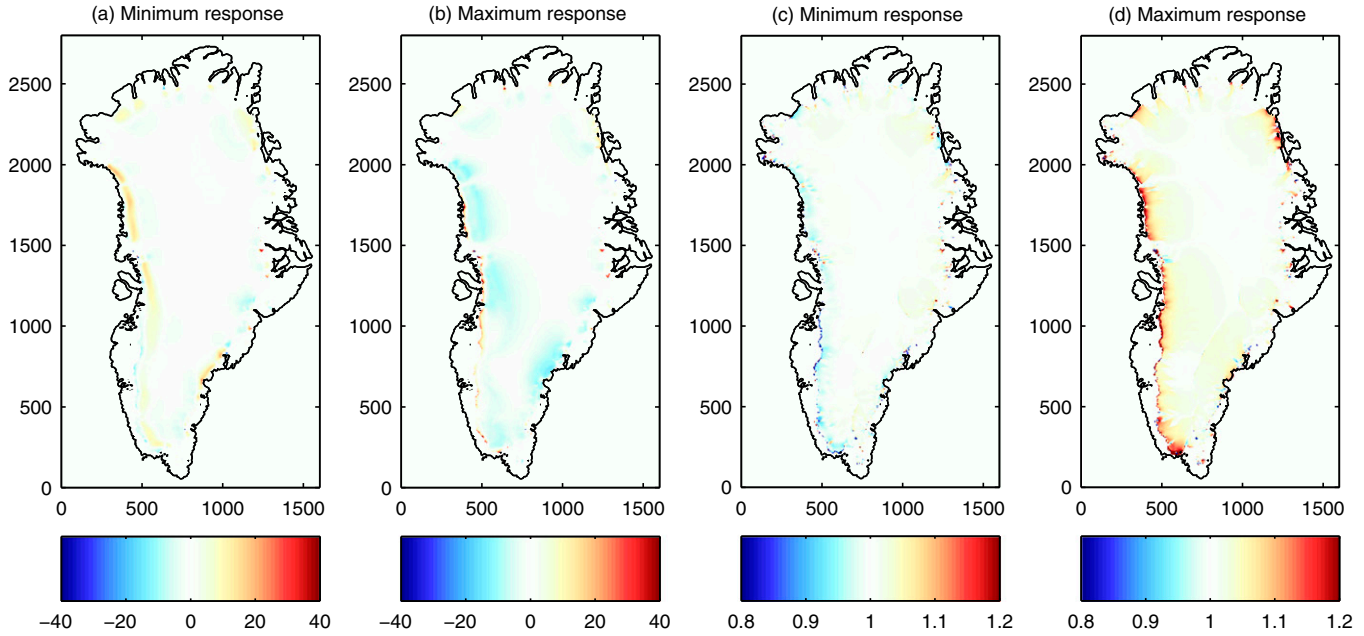

Fig. S2. (*A–D*) The pattern of additional thickness change generated by enhanced lubrication by the VUB-GISM-HO model in (*A*) RUN0002 and (*B*) RUN1026 (mean for 2190–2199 differenced against SMBONLY) and pattern of velocity change again for (*C*) RUN0002 and (*D*) RUN1026 (expressed as ratio to SMBONLY velocity).

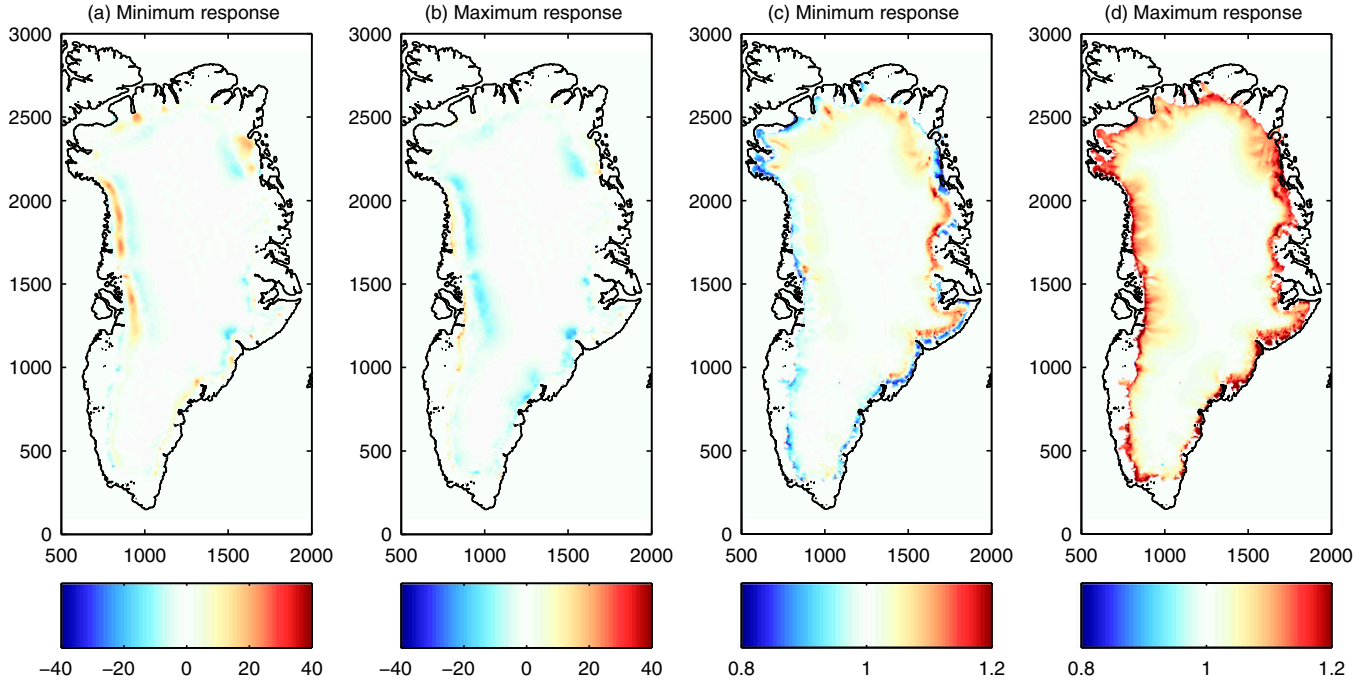

Fig. S3. (*A–D*) The pattern of additional thickness change generated by enhanced lubrication by the Elmer/Ice model in (*A*) RUN0002 and (*B*) RUN1026 (mean for 2190–2199 differenced against SMBONLY) and pattern of velocity change again for (*C*) RUN0002 and (*D*) RUN1026 (expressed as ratio to SMBONLY velocity). Note that results have been projected onto a 5-km grid and do not show all of the detail of the original finite-element grid.

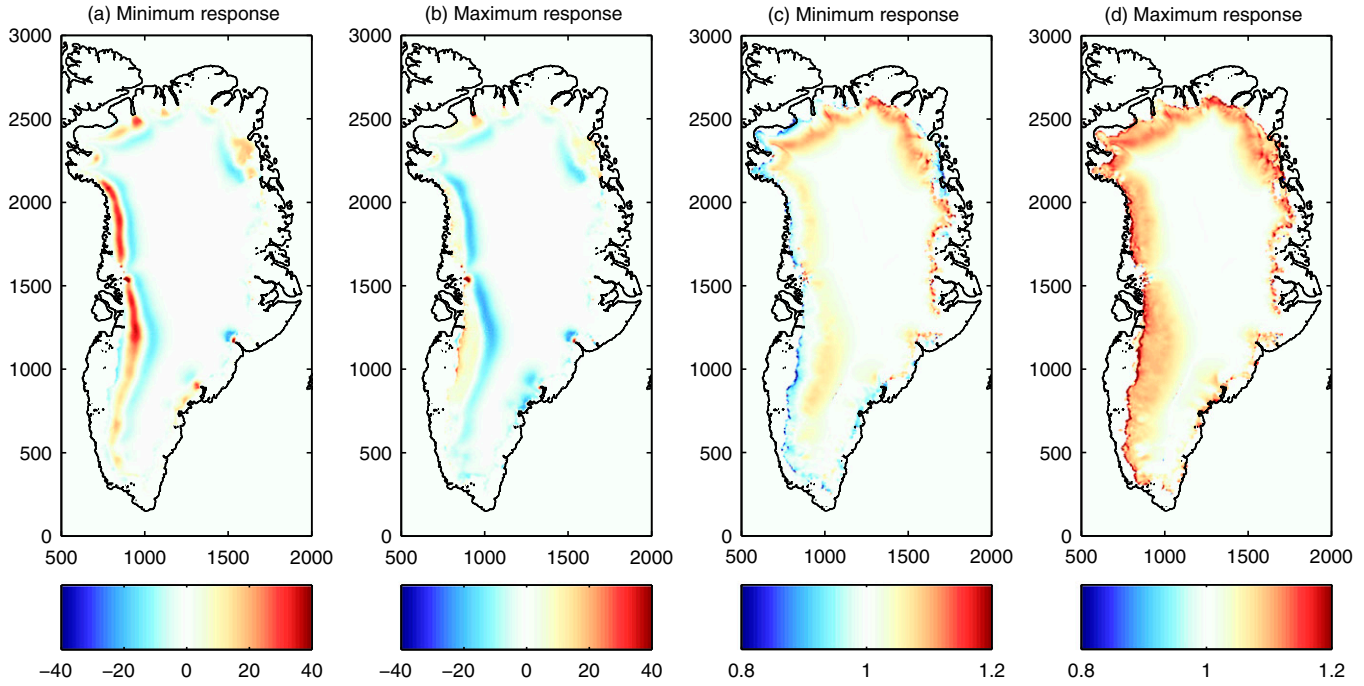

Fig. S4. (*A*–*D*) The pattern of additional thickness change generated by enhanced lubrication by the MPAS-Land Ice model in (*A*) RUN0002 and (*B*) RUN1026 (mean for 2190–2199 differenced against SMBONLY) and pattern of velocity change again for (*C*) RUN0002 and (*D*) RUN1026 (expressed as ratio to SMBONLY velocity).